Signal model of a cycloidal drive for diagnostic purposes

P. Grosso [1], **G. Massaccesi** [2], **J. Cavalaglio Camargo Molano** [2], **G. Mottola** [1], **D. Borghi** [2]
[1] University of Modena and Reggio Emilia, Department of Sciences and Methods for Engineering,
Via G. Amendola 2, 42122 - Reggio Emilia, Italy
e-mail: **pasquale.grosso@unimore.it**

[2] Tetra Pak Packaging Solutions,
Via A. Delfini 1, 41123 - Modena, Italy

Abstract
The study of gearboxes for diagnostic and prognostic purposes plays a major role in industrial applications, especially in the robotics and automation fields, where such devices are used extensively. The present work has been focused on the cycloidal drives, which are widely adopted thanks to their compactness and sturdiness, nevertheless they present a complex architecture. An analytical model of the vibrational behaviour of such a device has been developed aiming to obtain an efficient simulation tool, able to consider different faults occurring due to the natural wear of components. The model has been obtained thanks to a positional angular-based method giving the contacts patterns construction as a time-independent function, thus any input speed profile can be taken into account. Internal loads distribution has been a crucial aspect of the modelling, also needed in order to provide an estimate of the machine efficiency. This simulation tool may be finally generalized in order to extend the analysis capability to the epicyclic gear train family.

1 Introduction

In the industrial automation field, particularly in precision motion control, the *cycloidal* drives or speed reducers, also known as *cycloid* drives (often shortened in *cyclo*-drives) are a family of reduction gear mechanisms largely adopted thanks to several advantages including: reduced size even with high reduction ratios, about zero backlash, high torsional rigidity. As shown in Figure 1, a typical cycloid drive consists of an eccentric high speed shaft (having one or more cranks, depending on the number of discs present) installed in the case by means of two "classical" bearings, one or more planet cycloid wheels (discs) meshing with cylindrical pins mounted on an external fixed ring, and an output flange which incorporates pins engaging with planet wheels eyelets through hollow rollers. The planet discs are characterized by an epitrochoid profile, a curve belonging to the cycloids family. The operating principle is based on a first conversion of the rotary motion of the input shaft into the orbital one of the discs thanks to the presence of the cranks (one for each disc and oriented in a way which makes them angularly equidistant), the discs having holes arranged on a circumference and equidistant from each other, in turn they engage the output flange by means of the rollers which move on a circumference integral to the output flange, making its motion of a rotary type again but the direction turns to be opposite with respect to the input shaft one (see Figure 2): in this way the speed reduction is accomplished. The reduction *ratio formula* can be obtained by seeing the *cyclo*-drive as an epicyclic gear train (see Figure 2), where the related fixed carrier train *ratio* leads to:

$$\tau_0 = \frac{\omega_D}{\omega_{HG}} = \frac{Z_{HP}}{Z_L} \tag{1}$$

being ω_D and ω_{HG} the angular velocities of the disc and housing gear respectively, while Z_{HP} is the number of the housing pins and Z_L is the number of the disc lobes. Letting ω_C be the angular velocity of the carrier, since the present gear train sees $\omega_{HG} = 0$, the reduction *ratio* can be derived from the Willis *formula* as follows:

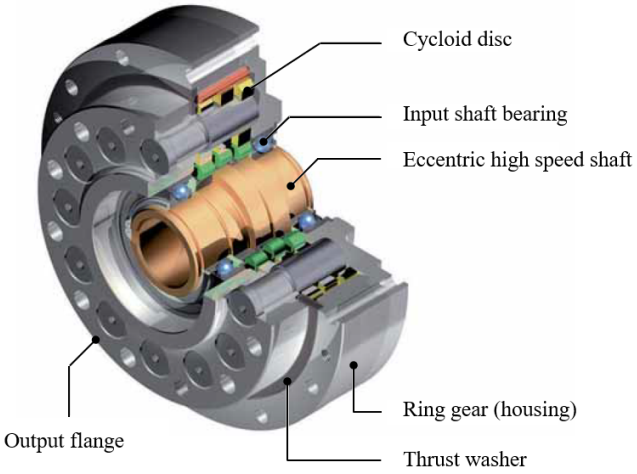

Figure 1: cycloidal drive made by Sumitomo (FC-A series), courtesy of *Sumitomo Drive Technologies*

$$\tau_{0'} = \frac{\omega_D - \omega_C}{-\omega_C} = 1 - \frac{\omega_D}{\omega_C} = \frac{Z_{HP}}{Z_L} = \tau_0 \tag{2}$$

$$\therefore\ \tau = \frac{\omega_D}{\omega_C} = 1 - \tau_0 = 1 - \frac{Z_{HP}}{Z_L} = -\frac{Z_{HP} - Z_L}{Z_L} \tag{3}$$

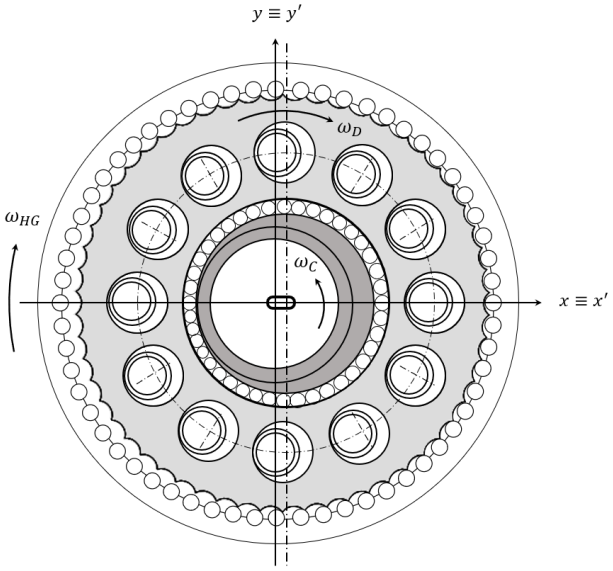

Figure 2: cycloidal drive operating scheme

Scientific literature includes several works on *cyclo*-drives, most of them, however, are focused on the operating principles, the analytical methods for the tooth profile generation and the computation of forces acting among the internal elements. Kudrijavcev [1] studied the cycloid drives functioning principles in details. Litvin and Feng [2] gave a fundamental contribution on the modelling of the cycloid disc tooth-profile generation, while Chmurawa and Lokiec [3] proposed an interesting tooth-profile disc modification. Dizioglu [4] discussed the formal problem of the cycloids family singularity points, in a continuous transition point of view. Blanche and Yang [5] studied the effects of machining tolerances on backlash and torque ripples. Yan and Lai [6] studied a geometry design of an elementary planetary gear train with cylindrical tooth-profiles by applying the envelope theory to derive the surface equation. Hwang and Hsieh [7] adopted the gearing theory to derive the mathematical model of an internal cycloidal gear with tooth difference, providing designs for both a gerotor and a speed reducer. On the other hand, an important pioneering work on the computation of forces acting among the internal elements of such devices, is owed to Lemhann [8], while Malhotra and Parameswaran [9] presented a procedure to calculate the theoretical efficiency, having computed the internal forces. Gorla et al. [10] developed an innovative *cyclo*-drive, modelling the contact loads and the machine efficiency, while Thube and Bobak [11] used 3-dimensional finite element analysis in order to investigate with more accuracy the load distributions on a cycloid disc. Sensinger [12] developed a model based on a unified set of equations in order to optimise the design of cycloid discs taking into account several aspects such as backlash, torque ripple, and reduction *ratio*. By contrast, not much has been produced regarding the condition monitoring issue, applied to cycloidal speed reducers. By the way, the work of Bechhoefer [13] is montioned, which proposes a modeling required for correct configuration to perform such analysis and documents the sensitivity of standard condition indicators for gear/bearing during the run to failure test. Finally, Cochran and Bobak [14], from Sumitomo Drive Technologies identified some frequencies to be monitored, showing tresholds amplitudes variation due to experimentally injected faults.

The present analysis adopts, as a reference model, the *Fine Cyclo* FCA 25G 29 made by Sumitomo Drive Technologies company, whereas the main constructive parameters are reported in the Table 1. Apart from the present introduction section, the work is structured as follows: in Section 2, the vibration signal general model, which is based on characteristic frequencies [15], is presented, starting from a well-established equation developed to describe the vibration signal of a localized fault occurring in the bearings [16]. Then the analytical model building algorithm is summarized in its steps, where the main aspect is represented by transposition of the purely time-depending characteristic frequencies in the angular domain, making them functions of the time by means of an angular coordinate, allowing to take into account any motion profile of the input shaft. Since the model adopts a SDOF impulse response as a filter function, its parameters must to be identified. Hence, in this regard, a numeric procedure is proposed. Section 3 is focused on the internal loads distribution computation, following as the outline, the approach adopted by Gorla et al. [10] and related to an innovative cycloid drive having however a single disc, whereas the present case is more complex since a 3-discs *cyclo* drive is studied: some simplifying hypotheses are considered, among which the strongest concerns the neglect of sliding and friction effects. Then, a machine efficiency estimate is provided, which can be useful in order to make some assessments, thanks to experimental evidence (input torque monitoring), about the power loss due to lubricant degradation and increasing wear. In Section 4 are reported some simulation output *spectra*, where both a constant and a customized velocity profiles, as input data, are taken into account. The latter case has required an order analysis, since the frequency one turns out to be an ineffective tool. Finally, Section 5 offers some conclusions and suggestions for further developments and future work.

Table 1: Sumitomo *Fine Cyclo* FCA 25G 29: some constructive parameters

Symbol	Description	Value
Z_D	no. of discs	3
Z_L	no. of lobes for each disc	58
Z_{HP}	no. of housing pins	60
Z_{OR}	no. of output rollers	12
τ	reduction *ratio*	29
e	eccentricity	$1\mathrm{e}{-3}$ [m]
ϕ	eccentricity directions phase shift	$(2/3)\pi$ [rad]

2 Analytical model of the vibration signal

2.1 Introduction

The development of the model is based on a step-by-step construction of a time array skeleton, which is mathematically represented by a binary output vector, where each component represents a time sample and can therefore assume the value 1, if that given instant of time contemplates an impulsive nature event borrowed from the physical reality of the problem, zero otherwise. These events can identify some dynamic characteristics of the system in its proper functioning, or even characteristics of a damaged system. Since the device under analysis is characterized by a no backlash functioning, the incipient fault is commonly caused by fatigue and wear due to several friction and sliding contacts which take place continuously during the operation, *i.e.* some internal elements may be affected by a local loss of material (spalling, pitting, etc...). Whenever an element of the *cyclo* impacts on a damaged part, it is possible to detect a load fluctuation that excites a system structural resonance and the vibration sensor one (if the latter is present). The repetition of the impacts produces a series of impulses that depends on the rotational velocity and on the geometry of the object. The amplitude of the vibration signals depends on the wear state of the damaged part, the load applied and the position of the internal elements. As regards the bearings, this has been established [17], and it is expected that is also valid for devices such as the one under analysis. The vibration signal of a localized fault occurring in the bearings is modelled as follows [16]:

$$x(t) = \sum_{i=-\infty}^{\infty} h(t - iT - \tau_i)q(iT) + n(t) \tag{4}$$

where, with reference to the present study case, $h(t)$ is the impulse response due to the impact on the damage point, T is the interval between two consecutive impacts due to a specific type of damage, $q(iT)$ is the modulation of the signal produced by the load distribution, τ_i takes into account the uncertainties due to the random slipping[1] of the rollers (housing or output ones), $n(t)$ is the background noise and i is the integration time step (time samples index).

It can be hypothesized that damages may affect the housing ring pins, the lobes of the discs or the output rollers, as well as the elements of the bearings present in the *cyclo* which, however, are not taken into account in this discussion. Therefore, letting $f_{rot,IS}$ be the rotational frequency of the input shaft, being interested in housing pin fault, in addition to the rotational frequency itself, the other to be monitored is the mesh one [14], whose expression is the following:

$$f_m(\lambda) = \lambda \times Z_{HP} \times f_{rot,IS}, \quad \lambda = 1, 2, 3 \tag{5}$$

where, since the housing pins have interactions with all discs and a fault can occur along a portion falling between ~ 0 and the entire length of the pin, f_m is placed as function of the index λ in order to take into account the possibility that the fault area may have interaction with $1, 2$ or 3 discs. A possible damage affecting a disc lobe is related to the rotational frequency of the disc itself (*i.e.* the output flange rotational frequency $f_{rot,OF}$) given by:

$$f_D = f_{rot,OF} = \tau \times f_{rot,IS} \tag{6}$$

Finally, since the output rollers motion is marked by $f_{rot,IS}$ (being ideally the contact given by output roller and eyelet of the disc a rigid connection running as the input shaft eccentric bearing) and they are constantly in contact with all discs, same considerations made about the pins are valid, thus a possible fault related to such elements may be detected by monitoring the $f_{rot,IS}$ as a function of λ, then:

$$f_{OR}(\lambda) = \lambda \times f_{rot,IS} \tag{7}$$

[1] However, this term is not object of the present discussion.

2.2 Model building

Borrowing the approach adopted by Molano et al. [15] for a case study application of the bearing fault, the procedure consists of the steps listed below.

1. Define an n-components vector **x** filled with zeros representing the expected vibration signal recorded by a sensor placed on the *cyclo* housing. Each cell of the vector corresponds to the time sample: $t_i = 1/f_s$, where f_s is the sampling frequency of the sensor [Hz].

2. Resample the defined motion profile $\theta(t_i), i = 1, 2, ..., n$ and the zero-initialized load vector $\mathbf{q}(t_i)$ at the sensor sampling frequency f_s.

3. Replace 1 in the cells of vector **x**, which index values are defined according to the periodical "events" and faults to be taken into account. Being the latter related to the frequencies presented in the previous section, in order to contemplate any motion profile of the input shaft, it is necessary to think in terms of (angular) position rather than time, *i.e.* two contacts involving the same "damaged" element are thought as located at the edge of a certain angle $\Delta\theta$, being known the angular motion law of the input shaft $\theta(t_i)$. Then, since Θ denotes an input shaft complete rotation, one has:

$$\Delta\theta_{HP}(\lambda) = \Delta\theta_{OR}(\lambda) = \Theta/\lambda \tag{8}$$

$$\Delta\theta_{MF}(\lambda) = \Theta/(\lambda\, Z_{HP}) \tag{9}$$

$$\Delta\theta_{DL} = \Theta\frac{\tau+1}{\tau} \tag{10}$$

   where in Eq. (8) considering an housing ring fault, $\Delta\theta_{HP}$ is the angle between two faulty contacts (expressed as function of λ, see previous section), as considering an output roller fault, $\Delta\theta_{OR}$ is the angle among two matches between a roller external surface defect and a disc (or more discs, depending on the defect extension) eyelet. Eq. (9) provides the angle between two contiguous contacts due to the gear mesh, and finally considering a disc lobe damaged, it impacts on two non-adjacent pins spaced according to the Eq. (10).

4. Weight the vector **x** by means of the load vector **q** computed according to the procedure explained in the Section 3.

5. Filter the generated vector **x** by means of an FFT-based technique using overlap-add method [18], where the filter function is the second derivative[2] of a SDOF system impulse response. This type of filtering is based on the principle that the multiplication in the frequency domain is equal to the convolution in the time domain. It operationally consists of the following phases:
   - transposition of the input "time" signal (in this case vector **x**) into the frequency domain through the FFT;
   - multiplication of the result obtained from the previous operation by the frequency response of the filter function (in this case the impulse response of a SDOF system);
   - transposition of the result into the time domain by using the inverse FFT.

   The generated response of a SDOF system to a unit impulse in time domain is given by:

$$x_{SDOF}(t) = h(t) = \frac{1}{m\omega_d} e^{-\zeta\omega_n t}\sin\omega_d t \tag{11}$$

   where m is the mass system, ζ is the damping ratio, and $\omega_d = \omega_n(1-\zeta^2)^{1/2}$ is the damped angular frequency while ω_n is the undamped one.

In order to simulate multiple faults at the same time, step 3 sees the recursive filling of the load vector, before vector **x** is weighted by it.

[2] Being the accelerometers, the typical vibration sensors adopted in experimental test.

2.3 Formalization of the optimization problem

In order to identify the SDOF system parameters, a numeric procedure may be adopted. The idea is to place the analytical expected signal equal to an experimental acquired one, thus, considering the Eq. (4), thanks to the following substitutions:

$$x(t) \to c(i), \quad h(t - iT - \tau_i)q(iT) \to y(i), \quad n(t) \to r(i) \tag{12}$$

it can be rewritten, as a fully discrete form problem, leading to n equations of the following type:

$$y(i) + r(i) = c(i), \quad i = 1, 2, ..., n \tag{13}$$

where, since n is the number of time samples, $c(i)$ is the i-th time sample of the "real" signal, $r(i)$ is the i-th component of a random noise array, while $y(i)$ is the i-th component of the operator relation output, giving by the filtering of the analytically built signal through the impulse response second derivative of the SDOF system. Then, $y(i)$ can be expressed as follows:

$$y(i) = \sum_{j=1}^{n_s} s(j)x(i - j + 1), \quad \begin{cases} x(i - j + 1), & i \geq j \\ 0, & i < j \end{cases} \tag{14}$$

being $s(j)$ the j-th discrete value of the SDOF system impulse response (second derivative) and $x(i-j+1)$ the $(i - j + 1)$-th component of the analytically built signal array. Finally, n_s is the filter length, which can be also placed equal to n. A compact form of $s(j)$ can be given by the following expression:

$$s(j) = Ae^{-\zeta\omega_n t(j)}[B \sin(\omega_d t(j)) + C \cos(\omega_d t(j))], \tag{15}$$

$$\begin{cases} A = \omega_n^3/k \\ B = \frac{2\zeta^2-1}{(1-\zeta^2)^{1/2}} \\ C = 2\zeta \end{cases} \tag{16}$$

where $\{\omega_n, \zeta, k\}$ is the set of problem unknowns, which, as can be seen, are not j-depending (unlike time variable: time discretization). By placing, for sake of compactness:

$$p(i) = c(i) - r(i) \tag{17}$$

after operating the following change of notation: $\alpha(i) \equiv \alpha_i$ and taking into account the case: $n_s = n$, the system given by Eqs. (10) can be rewritten as follows:

$$\begin{pmatrix} x_1 & 0 & & \cdots & & 0 & 0 \\ x_2 & x_1 & & \cdots & & 0 & 0 \\ \vdots & \vdots & \ddots & & & \vdots & \vdots \\ x_k & x_{k-1} & \cdots & x_1 & \cdots & 0 & 0 \\ \vdots & \vdots & & & \ddots & \vdots & \vdots \\ x_{n-1} & x_{n-2} & & \cdots & & x_1 & 0 \\ x_n & x_{n-1} & & \cdots & & x_2 & x_1 \end{pmatrix} \begin{pmatrix} s_1 \\ s_2 \\ \vdots \\ s_k \\ \vdots \\ s_{n-1} \\ s_n \end{pmatrix} = \begin{pmatrix} p_1 \\ p_2 \\ \vdots \\ p_k \\ \vdots \\ p_{n-1} \\ p_n \end{pmatrix} \tag{18}$$

$$\therefore \ \mathbf{Xs} = \mathbf{p} \ \therefore \ \mathbf{s} = \mathbf{X}^{-1}\mathbf{p} \tag{19}$$

where the latter is an overdetermined non-linear system in the unknowns, therefore its resolution can be attempted through a numerical technique. The limit is represented by the analytically building signal, which, before the filtering operation, is in the form of a sparse-array.

3 Internal loads distribution

3.1 Introduction

The entire section shows a method for estimating the contact forces among the internal elements of the gearbox. Following the approach of Gorla et al. [10], some assumptions are taken into account:

- perfect geometry;
- rigid bodies;
- negligible friction and weight[3].

Considering, for sake of simplicity, the presence of a single disc [4], and therefore a single disc holder bearing, its eccentricity with respect to the input shaft section is supposed to be lying on the x-axis (see Figure 3.(a)).

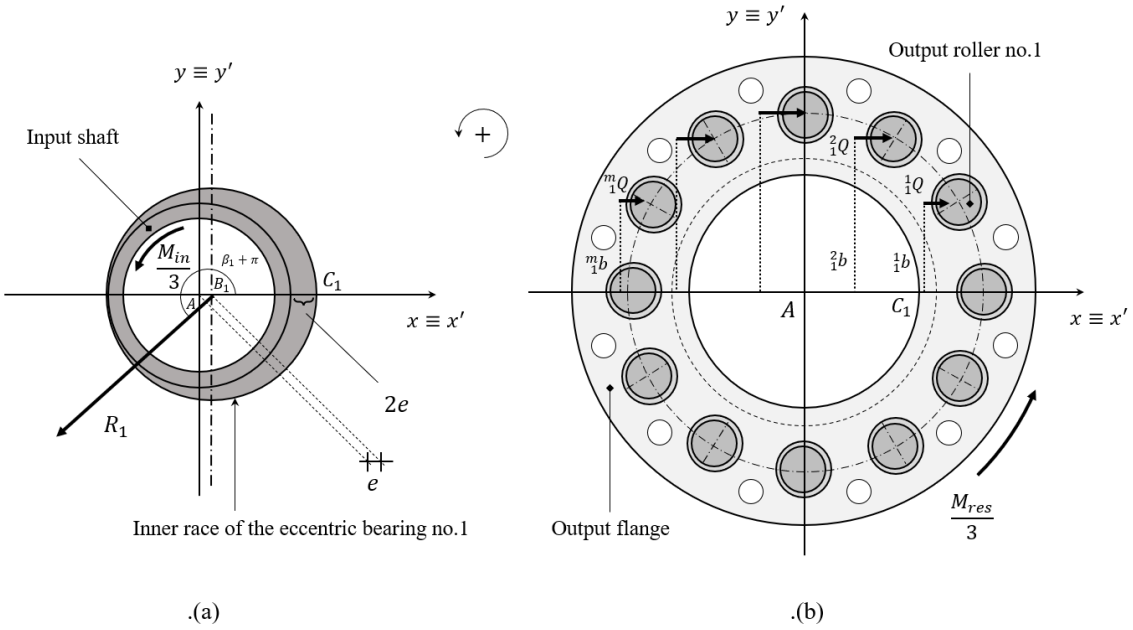

Figure 3: torque equilibrium along the axial direction: input .(a), output .(b) sections

Since the input torque is split among the three eccentric bearings which inner races are as one with the main body of the input shaft holder sleeve [5], the torque equilibrium of the input shaft may be expressed by the following equation (referring to the Figure 3.(a)):

$$\frac{M_{in}}{3} + eR_1 \sin(\beta_1 + \pi) = 0 \tag{20}$$

hence:

$$\frac{M_{in}}{3} - eR_1 \sin(\beta_1) = 0 \quad \therefore \quad R_1 = \frac{M_{in}}{3e \sin(\beta_1)} \tag{21}$$

where R_1 is the crank reaction due to the disc no.1, M_{in} is the input torque, e is the eccentricity, and β_1 identifies the angular position of R_1 direction.

[3]The gearbox is considered having the axis in vertical position.

[4]In this regard, the discussion uses the numerical assignment with value 1, with reference to the cardinality of the set of eccentric bearings and of the relative discs.

[5]For the purposes of this discussion, the sleeve identifies the input shaft.

On the other hand, the torque equilibrium of the output flange contemplates a resistant torque which has the direction of rotation as shown in the Figure 3.(b), since the device reverses the direction of rotation; the resistant torque is counterbalanced by the reactions acting in the contacts among the flange eyelets and the output rollers. Although contacts take place between all the eyelets and relative output rollers, nevertheless only some of them take part in torque transmission (remembering that just one disc is considered), since only compressive forces can be transmitted. The reason why the only forces involved are (ideally) those schematized in the Figure 3.(b) will be clarified later. Finally, the torque equilibrium is described by the following equation:

$$\frac{M_{res}}{3} = \sum_{j=1}^{m} {}^{j}_{1}Q \, {}^{j}_{1}b \tag{22}$$

where M_{res} is the resistant torque, ${}^{j}_{1}Q$ is the j-th force due to the presence of the disc no.1, and ${}^{j}_{1}b$ is its arm respectively.

3.2 Forces computation

The eccentric bearing, in its rotary motion, holds the disc to always be in contact with some housing pins and all internal output rollers. The "static" configuration in Figure 4, the one already seen with eccentricity direction coinciding with the x-axis, shows the contacts among the disc lobes and the housing pins on the entire right half-plane (where, since the housing pins are 60 and the lobes are 58, the pins involved in the contact turn out to be $58/2 = 29$). However, it must be borne in mind that if all these contacts generated forces, the disc would be self-balanced with respect to the vertical translation, when it is the vertical component of the crank reaction, to guarantee this balance. It follows that only the contacts which take place in the first quadrant produce forces, with the exception of the pin whose center lies on the x-axis, which represents a singularity.

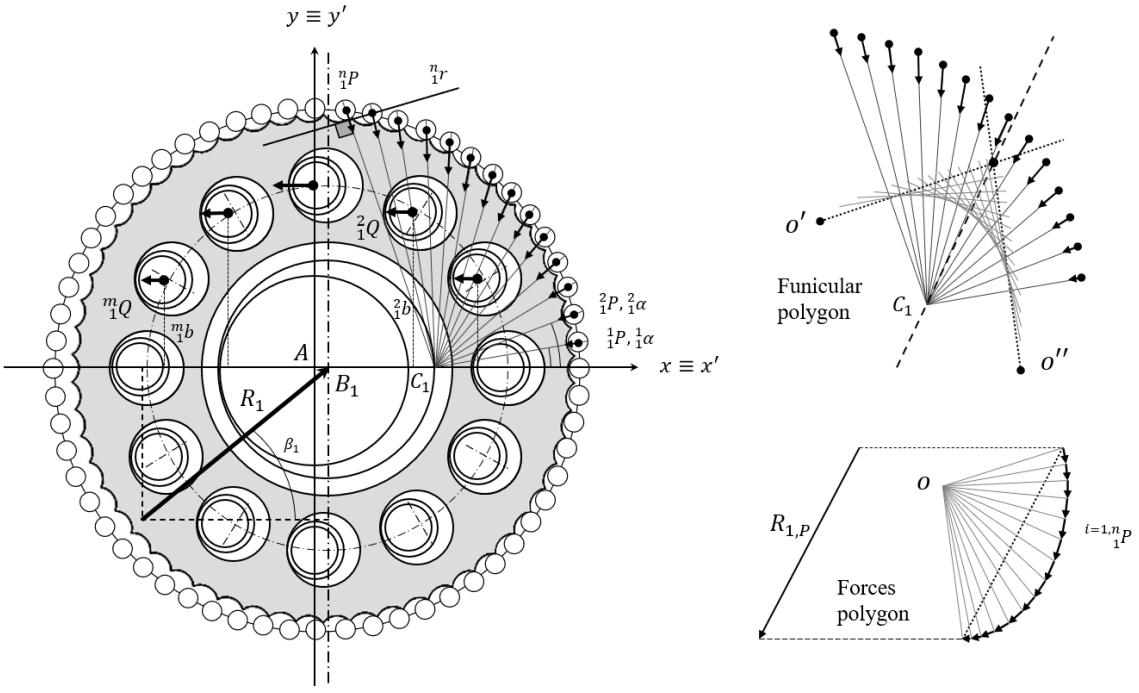

Figure 4: forces acting on the disc

Seeing the gear train as an epicyclic one (referring to the Figure 4), it is easy to observe that notable point C_1 represents the *instantaneous rotation centre* between the housing pins ring and the disc, thus all the directions

of the forces acting among the disc lobes and the housing pins, named ${}^{i=1,n}_{1}P$, converge in this point. Since $\overline{B_1C_1}$ is also the pitch *radius* of the disc, its calculation is based on the *modulus* definition, hence:

$$\mathrm{m} \triangleq \frac{d_{rg}}{Z_{HP}} = \frac{d_{pg}}{Z_L} \quad \therefore \quad \begin{cases} d_{rg} = \mathrm{m}Z_{HP} = m(Z_L + 2) \\ d_{pg} = \mathrm{m}Z_L \end{cases} \tag{23}$$

where d_{rg} and d_{pg} are the pitch diameters of the housing pins ring and of the disc respectively, and by placing eccentricity equal to the pitch *radii* difference:

$$e = \frac{d_{rg} - d_{pg}}{2} = \frac{\mathrm{m}}{2}(Z_L + 2 - Z_L) = \mathrm{m} \tag{24}$$

one obtains:

$$\overline{B_1C_1} = \frac{d_{pg}}{2} = \frac{\mathrm{m}}{2}Z_L = \frac{e}{2}Z_L \tag{25}$$

For the calculation of the ${}^{i=1,n}_{1}P$ reactions, it is necessary to consider the equilibrium in the y direction of the disc, which leads to the following equation:

$$R_1 \sin(\beta_1) - \sum_{i=1}^{n} |\,{}^{i}_{1}P \sin({}^{i}_{1}\alpha)| = 0 \tag{26}$$

where ${}^{i=1,n}_{1}\alpha$ are the angles between the x-axis and the segments $\overline{{}^{i}_{1}PC_1}$ respectively. Since the physical system is statically indetermined, the equations which describe the rigid body equilibrium of the disc in the plane, including Eq. (26), are not sufficient to completely determine every force. To solve the problem without taking it into account elastic compliance, the assumption that the modules of the ${}^{i=1,n}_{1}P$ forces have a sinusoidal distribution in the angular development of the first quadrant, is adopted [3, 9], leading to:

$$|\,{}^{i}_{1}\mathbf{P}| \propto |\sin({}^{i}_{1}\alpha)| \quad \therefore \quad |\,{}^{i}_{1}\mathbf{P}| = P_1 |\sin({}^{i}_{1}\alpha)| \tag{27}$$

whereas remembering the 2-nd of Eq. (20), ${}^{i=1,n}_{1}P$ expressions may be determined as:

$${}^{i}_{1}P = \frac{M_{in}|\sin({}^{i}_{1}\alpha)|}{3e\sum_{i=1}^{n}\sin^2({}^{i}_{1}\alpha)} \tag{28}$$

while the expression of the generic ${}^{k}_{1}\alpha$, with reference to Figure 5, is given by:

$${}^{k}_{1}\alpha = \arccos\left[\frac{h\cos({}^{k}_{1}\theta) - \frac{e}{2}Z_L}{\sqrt{(h\cos({}^{k}_{1}\theta) - \frac{e}{2}Z_L)^2 + h\cos({}^{k}_{1}\theta)^2}}\right] \tag{29}$$

On the other hand, for the computation of ${}^{j=1,m}_{1}Q$, it must be taken into account the torque equilibrium of the disc, whereas, as shown in Figure 4 in addition to the aforementioned forces, also the vertical components of both the crank reaction and the resultant of ${}^{i=1,n}_{1}P$ (named $R_{1P}|y$) contribute to the torque balance (while the horizontal component of the ${}^{i=1,n}_{1}P$ resultant, *e.g.* $R_{1P}|x$, since its direction lies on the x-axis, it has no role in the equilibrium). The equation is as follows:

$$\sum_{j=1}^{m} {}^{j}_{1}Q\,{}^{j}_{1}b - e(\frac{Z_L}{2} - 1)R_1 \sin(\beta_1) = 0 \tag{30}$$

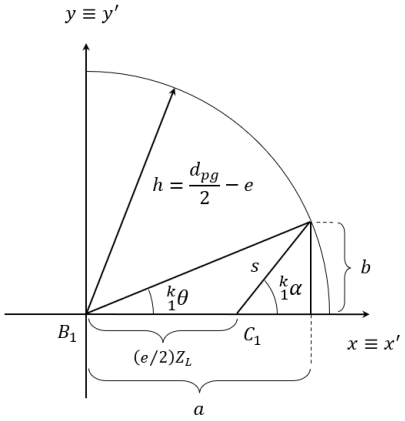

Figure 5: scheme for the computation of generic ${}^{k}_{1}\alpha$

where at this point, an assumption similar to the case of ${}^{i}_{1}P$ calculation is needed, *i.e.* the modules of the forces ${}^{j=1,m}_{1}Q$ are proportional to their arm ${}^{j=1,m}_{1}b$ [3, 9], leading to:

$$|{}^{j}_{1}\mathbf{Q}| \propto {}^{j}_{1}b \quad \therefore \quad |{}^{j}_{1}\mathbf{Q}| = Q_1 \, {}^{j}_{1}b \tag{31}$$

and remembering the 2-nd of Eq. (20), one reaches:

$${}^{j}_{1}Q = \frac{M_{in}}{3}\left[\left(\frac{Z_L}{2} - 1\right)\frac{{}^{j}_{1}b}{\sum_{j=1}^{m} {}^{j}_{1}b^2}\right] \tag{32}$$

Figures 6 and 7 show the typical result of the distributions of forces with $M_{in} = 9$ [Nm]. In Figure 6 the graphs refer to the case of a single disc, while taking into account also the two remaining ones, the distributions appear as shown in Figure 7, where as regards the P-type forces, the pattern referred to the single disc case is also repeated for the other ones with the exception of some pins among them which are completely discharged, this is because the configuration of the three discs is continuously such that the directions of the eccentricities lie on incident axes which are out of phase by 120 [deg], *i.e.* the load is symmetric with respect to an angular excursion of 120 [deg]. As for the Q-type forces, on the other hand, the interaction of the three discs modifies the appearance of the pattern resulting from the "presence" of a single disc.

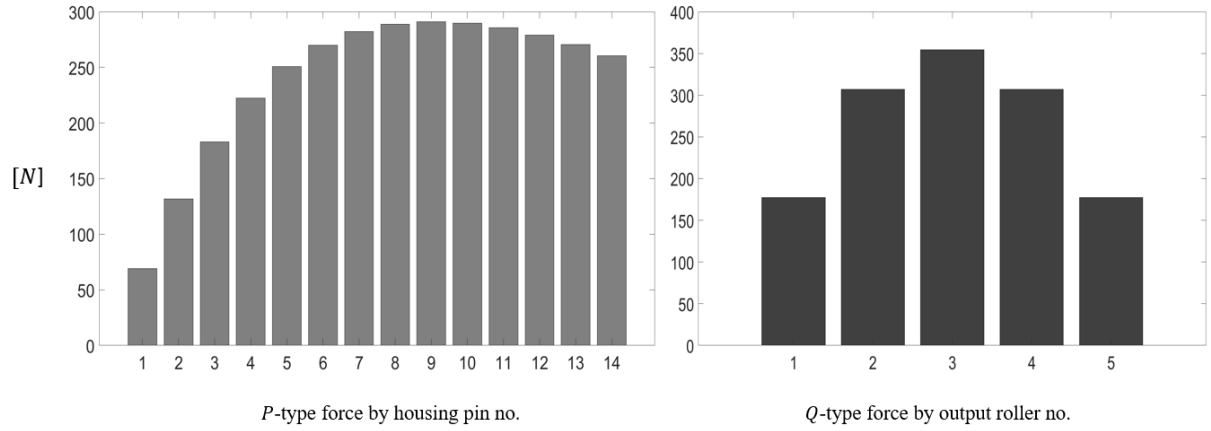

Figure 6: forces distributions referred to a simplified configuration including only one disc

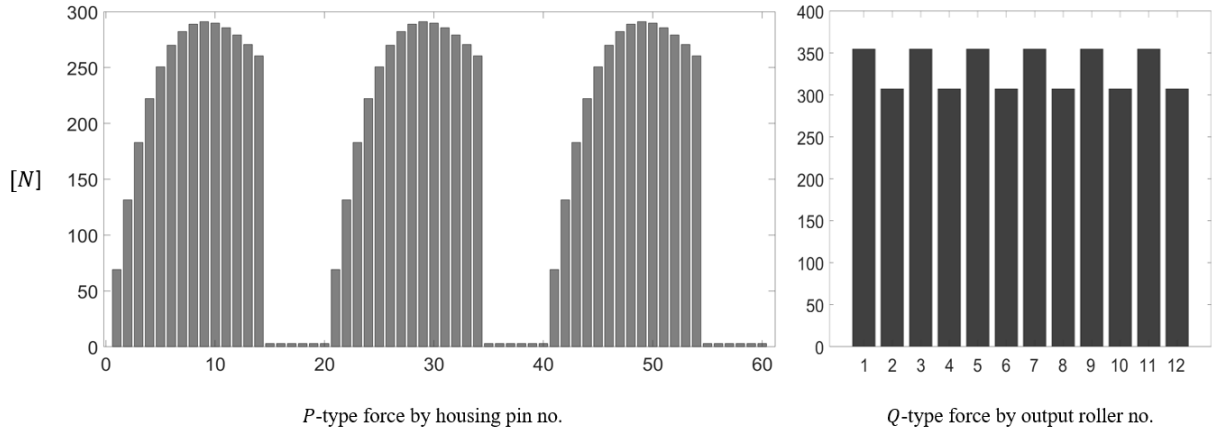

Figure 7: forces distributions referred to the standard configuration including all discs

3.3 Machine efficiency

By following the Malhotra method [9], which is more precautionary with respect to the Gorla's one [10], the power losses listed below are considered:

1. bearing friction in the mounting of the discs on the input shaft ($\rightarrow W_1$);
2. rolling contact friction between output rollers and eyelets in the discs ($\rightarrow W_2$);
3. rolling contact friction between housing pins and the discs ($\rightarrow W_3$);
4. bearing friction in the mounting of the output rollers ($\rightarrow W_4$);
5. bearing friction in the mounting of the housing pins ($\rightarrow W_5$).

Since $\mathrm{d}\theta$ is the infinitesimal rotation of the output flange, the related contributions to the frictional infinitesimal work are respectively given by the following expressions:

$$\begin{cases} \mathrm{d}W_1 = f_{r1}\gamma_1 \sum_{l=1}^{Z_D} R_l(\theta)\psi_1 \mathrm{d}\theta \\ \mathrm{d}W_2 = f_{r2} \sum_{l=1}^{Z_D} \sum_{j=1}^{m*} Q_{l,j}(\theta)\psi_2 \mathrm{d}\theta \\ \mathrm{d}W_3 = f_{r3} \sum_{l=1}^{Z_D} \sum_{i=1}^{n*} P_{l,i}(\theta)\psi_3 \mathrm{d}\theta \\ \mathrm{d}W_4 = f_{s1}\gamma_4 \sum_{j=1}^{m**} Q_j(\theta)\psi_4 \mathrm{d}\theta \\ \mathrm{d}W_5 = f_{s2}\gamma_5 \sum_{i=1}^{n**} P_i(\theta)\psi_5 \mathrm{d}\theta \end{cases} \tag{33}$$

, where f_{r1},f_{r2} and f_{r3} are the lever arms of rolling friction, while f_{s1} and f_{s2} are sliding friction coefficients. The constants γ_1, γ_4 and γ_5 are the *ratio* between the pitch diameter of the eccentric bearings and its rollers diameter, the output rollers *radius* and the housing ring pins *radius* respectively, while coefficients $\psi_{u=1,5}$ quantify the rotations of the elements involved in the $\mathrm{d}W_{u=1,5}$ contributions respectively, with respect to $\mathrm{d}\theta$ (where $\psi_1 = \psi_2 = \psi_4 = \tau^{-1}$). Finally, the values of the indices m^*, n^*, m^{**}, n^{**}, are the number of elements involved in the respective contributions $\mathrm{d}W_{u=1,5}$ with respect to the total of m and n respectively. The instantaneous efficiency is then:

$$\eta_i = \frac{M_{in}\tau^{-1}\mathrm{d}\theta - \sum_u \mathrm{d}W_u}{M_{in}\tau^{-1}\mathrm{d}\theta} \tag{34}$$

By integrating $\mathrm{d}W_{u=1,5}$ contributions over the duration of one rotation of the input shaft, *i.e.* $2\pi\tau$ rotation of the output flange, the overall efficiency can be expressed as follows:

$$\eta_o = \frac{M_{in}2\pi - \int_0^{2\pi\tau} \sum_u \mathrm{d}W_u}{M_{in}2\pi} \tag{35}$$

4 Simulation output

4.1 Constant velocity profile

This section deals with the first of the two analytically built signal examples, where in this case a constant input shaft rotational speed is considered. A possible output of a hypothetical accelerometer fixed on the *cyclo*-drive case, with a radial acquisition axis is shown in Figure 8 in terms of the signal frequency *spectrum* while in Table 2 the values of the adopted parameters and the expected frequencies are shown (it is arbitrarily choosen to consider only the rotation and mesh frequencies). These parameters must be tuned starting from a set of experimental data, following for example the procedure proposed in Section 2.3. Furthermore, to validate the simulation tool, it would be advisable to calibrate the amplitude thresholds of the peaks identifying the frequencies to be monitored, on the basis of the experimental data, first adopting nominal load and a "healthy" machine, then adopting same worn one, which will require greater input torque (a parameter which represents an input data for the simulation), with the same output one due to the higher dissipation. Here, the load vector $\mathbf{q}$ was generated with a simplified procedure by adopting the maximum value among those of the forces acting between the housing ring pins and the lobes of the discs (${}^{i=1,n}_{1}P$, see Section 3.2), this value is present recursively in $\mathbf{q}$ with a periodicity related to the mesh frequency, while concerning the rotational frequency the load value adopted is given by $M_{in}/3/e$. Finally, since each variation of the mechanical system configuration leads to different results in terms of signal output, keep in mind that tuning operations must be carried out for each new configuration taken into account.

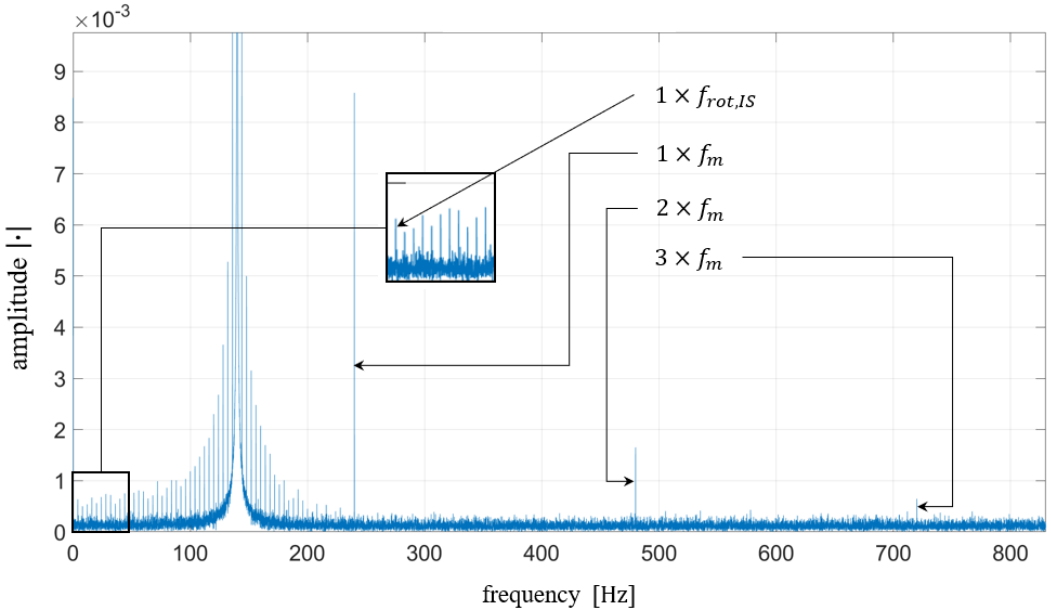

Figure 8: frequency *spectrum* of the simulated vibration signal

Table 2: simulation data

adopted parameter	value	output frequency	value
f_n	140 [Hz]	$1 \times f_{rot,IS}$	4 [Hz]
ζ	5e−4	$1 \times f_m \equiv f_m(1)$	240 [Hz]
k	2e13 [Nm^{-1}]	$2 \times f_m \equiv f_m(2)$	480 [Hz]
$n = n_s$	4e5	$3 \times f_m \equiv f_m(3)$	720 [Hz]
$f_s = 2e4$ [Hz]	$M_{in} = 9$ [Nm]	$SNR = 0$	

4.2 Customized velocity profile

Thanks to position-based model building (see Section 2.2), it is possible to obtain signal output simulations where any motion (velocity) profile of the input shaft can be taken into account. Hence, the customized non-trivial profile shown in Figure 9 is considered in this session.

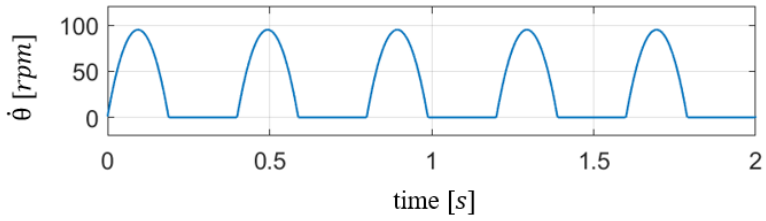

Figure 9: velocity profile pattern

Since a "traditional" frequency domain investigation is not very interesting in this case because the graph would be poor in information we are searching for, it is necessary to use a homologous analysis tool able to provide a *spectrum* which neatly show peaks relating to the significant events characterizing the simulation. Hence, an order analysis is performed, where a certain order represents the frequency with which an event occurs along a complete rotation of a reference point or element (in this case, the input shaft). A dummy accelerometer fixed on the *cyclo*-drive case with a radial acquisition axis is considered again, giving, as the simulation output, the order map shown in Figure 10. The waterfall plot sees the order numbers along the x-axis, the time axis as the y-axis and the RMS amplitudes along the z-axis. Since the graph does not present variation along the time axis, a more interesting projection in the x-z plane, named order *spectrum*, is displayed in Figure 11, showing the expected order numbers of the simulation. Letting ON_{ep} and $MON(\lambda)$ be the order number related to the elementary pattern repetition and to the meshing contacts one respectively (where λ assumes the meaning which was presented in Section 2.1), they clearly appear in Figure 11 where some harmonics are also present. The values of the adopted parameters and the expected orders are reported in Table 3, being considered, similarly to the previous case, only the orders related to the input shaft rotation and to the mesh contacts. The load vector $\mathbf{q}$ was here generated following the same simplified procedure adopted in the previous case, and also the same considerations made regarding the parameters tuning and the assessment of the amplitude peaks thresholds by experimental comparison, remains valid.

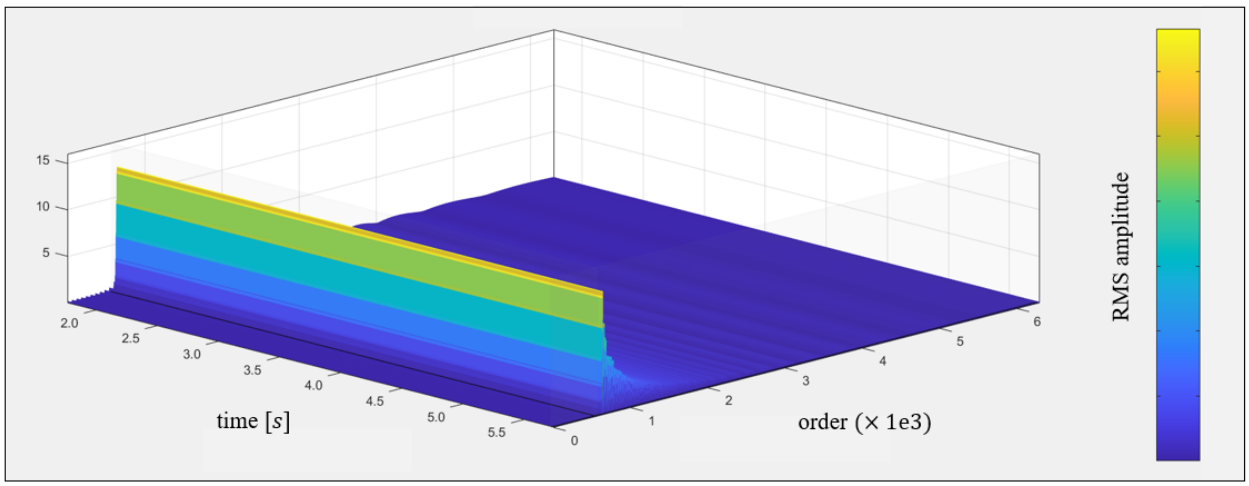

Figure 10: order map of the simulated vibration signal

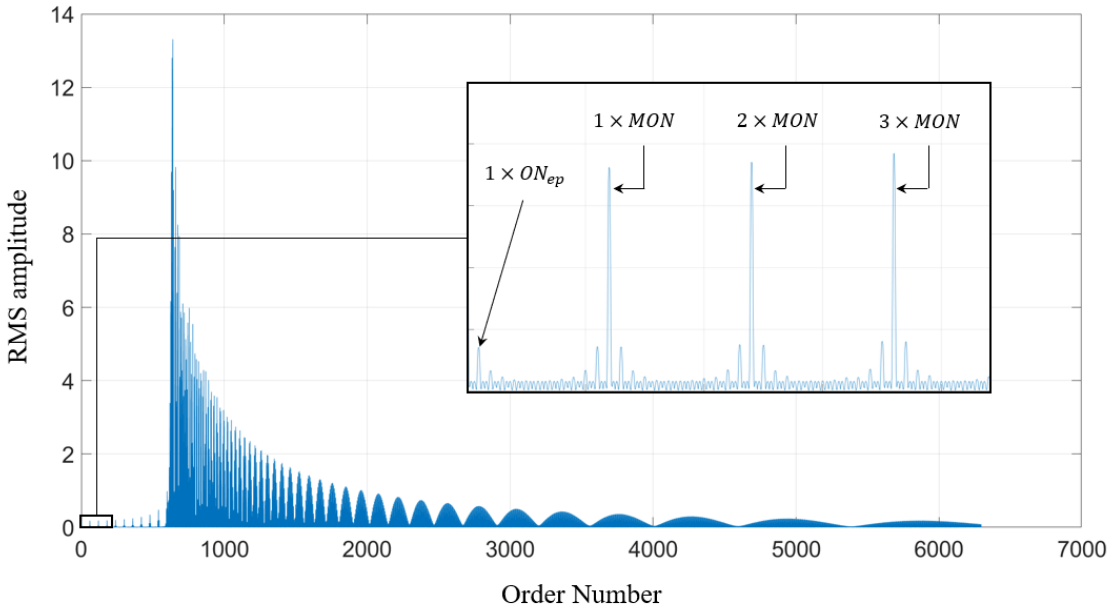

Figure 11: order *spectrum* of the simulated vibration signal

Table 3: simulation data

adopted parameter	value	output order numbers	value
f_n	1000 [Hz]	$1 \times ON_{ep}$	5
ζ	5e−4	$1 \times MON \equiv MON(1)$	60
k	2e13 [Nm^{-1}]	$2 \times MON \equiv MON(2)$	120
$n = n_s$	1.6e5	$3 \times MON \equiv MON(3)$	180
$f_s = 2e4$ [Hz]	$M_{in} = 9$ [Nm]	$SNR \to \infty$	

5 Conclusions

In the present work, a signal model of a cyloid drive, representing a possible output of an accelerometric sensor fixed on the running device, has been proposed. The model has been conceived for diagnostic purposes, since main characteristic "faults" frequencies has been identified and taken into account by the analysis. The internal load distribution computation has also been performed, whereas the model needed a load array in order to modulate the amplitude of the peaks generated due to the impulsive impacts simulating damages or significant periodical events characterising the running mechanical system. Thanks to the load distribution knowledge, it has been possible to provide a theoretical machine efficiency estimate, which can be useful to know the power decay mechanism, occurring due to lubrication degradation and then increasing wear. Some simulation output has been displayed for both constant and customized velocity profiles of the input shaft, where the latter case needed to be face by means of the order analysis technique, since the frequency analysis turns to be a not very effective tool. The simulation tool will must be refined according to experimental testing response, which can be useful both for identify some model parameters and for calibrate the amplitude thresholds of the peaks which significantly vary on general configuration of the mechanical system (layout, misalignment, load, environment). Apart from the last issue, further developments could be taken into account: such as the possibility of enriching the analysis by including sliding and frictioning effects, which occurs among the internal elements in contact. These effects are neglected here, since a modelling, given the complexity of the issue, has dignity to deserve a separate work, while it goes beyond the scope of the present one. Finally, the proposed signal model may also be adapted in order to simulate the vibrational behavior of any speed reducer belonging to the *epyciclic gear train* family, of which *cyclo*-drives represent a subset.

References

[1] V. Kudrijavcev, *Planetary gear train*. Leningrad, Russia: Mechanical Engineering, 1966 (in Russian).

[2] F. Litvin and P. Feng, "Computerized design and generation of cycloidal gearings," *Mechanism and Machine Theory*, vol. 31, no. 7, pp. 891–911, 1996.

[3] M. Chmurawa and A. Lokiec, "Distribution of loads in cycloidal planetary gear (cyclo) including modification of equidistant," in *Proceedings of the 16th European ADAMS User Conference*, Berchtesgaden,Germany, 2001.

[4] B. Dizioglu, "On the real singularities points of cycloids, epi- and hypocycloids," *Mechanism and Machine Theory*, vol. 21, no. 3, pp. 223–224, 1986.

[5] J. Blanche and D. Yang, "Cycloid driveswith machining tolerances," *ASME J. Mech., Trans., and Automation*, vol. 111, no. 3, pp. 337–344, 1989.

[6] H. Yan and T. Lai, "Geometry design of an elementary planetary gear train with cylindrical tooth profiles," *Mechanism and Machine Theory*, vol. 37, no. 8, pp. 757–767, 2002.

[7] Y. Hwang and C. Hsieh, "Geometric design using hypotrochoid and nonundercutting conditions for an internal cycloidal gear," *ASME Journal of Mechanical Design*, vol. 129, no. 4, pp. 413–420, 2007.

[8] M. Lehmann, *Calculation and measurement of forces acting on cycloid speed reducer, PhD Thesis*. Germany: Technical University Munich, 1976 (in German).

[9] S. Malhotra and M. Parameswaran, "Analysis of a cycloid speed reducer," *Mechanism and Machine Theory*, vol. 18, no. 6, pp. 491–499, 1983.

[10] C. Gorla, P. Davoli, F. Rosa, C. Longoni, F. Chiozzi, and A. Samarani, "Theoretical and experimental analysis of a cycloidal speed reducer," *ASME Journal of Mechanical Design*, vol. 130, no. 11, pp. 1 126 041–1 126 048, 2008.

[11] S. Thube and T. Bobak, "Dynamic analysis of a cycloidal gearbox using finite element method," *AGMA Technical Paper*, 2012.

[12] J. Sensinger, "Unified approach to cycloid drive profile, stress, and efficiency optimization," *ASME Journal of Mechanical Design*, vol. 132, no. 2: 024503, 2010.

[13] E. Bechhoefer, "Condition monitoring of a cycloid gearbox," in *Proceedings of the MFPT 2019*, Philadelphia, 2019.

[14] V. Cochran and T. Bobak, "A methodology for identifying defective cycloidal reduction components using vibration analysis and techniques," *AGMA Technical Paper*, 2008.

[15] J. Molano, L. Capelli, R. Rubini, D. Borghi, and M. Cocconcelli, "A bearing fault model for independent cart conveyor system and its validation," *Applied Acoustics*, vol. 159, 2020.

[16] P. McFadden and J. Smith, "Model for the vibration produced by a single point defect in a rolling element bearing," *Journal of Sound and Vibration*, vol. 96, no. 1, pp. 69–82, 1984.

[17] J. Gomez, A. Bourdon, H. André, and D. Rémond, "Modelling deep groove ball bearing localized defects inducing instantaneous angular speed variations," *Tribology International*, vol. 98, pp. 270–281, 2016.

[18] A. V. Oppenheim, R. W. Schafer, and J. R. Buck, *Discrete-Time Signal Processing, 2nd Edition*. Upper Saddle River, NJ: Prentice Hall, 1999.